

# Time-Dependent Activation of Feed-Forward Inhibition in a Looming-Sensitive Neuron

Fabrizio Gabbiani, Ivan Cohen and Gilles Laurent

*J Neurophysiol* 94:2150-2161, 2005. First published May 31, 2005; doi:10.1152/jn.00411.2005

**You might find this additional information useful...**

---

This article cites 33 articles, 20 of which you can access free at:

<http://jn.physiology.org/cgi/content/full/94/3/2150#BIBL>

This article has been cited by 5 other HighWire hosted articles:

**Influence of Electrotonic Structure and Synaptic Mapping on the Receptive Field Properties of a Collision-Detecting Neuron**

S. P. Peron, H. G. Krapp and F. Gabbiani  
*J Neurophysiol*, January 1, 2007; 97 (1): 159-177.

[\[Abstract\]](#) [\[Full Text\]](#) [\[PDF\]](#)

**Spike-Frequency Adaptation and Intrinsic Properties of an Identified, Looming-Sensitive Neuron**

F. Gabbiani and H. G. Krapp  
*J Neurophysiol*, December 1, 2006; 96 (6): 2951-2962.

[\[Abstract\]](#) [\[Full Text\]](#) [\[PDF\]](#)

**Role of an Identified Looming-Sensitive Neuron in Triggering a Flying Locust's Escape**

R. D. Santer, F. C. Rind, R. Stafford and P. J. Simmons  
*J Neurophysiol*, June 1, 2006; 95 (6): 3391-3400.

[\[Abstract\]](#) [\[Full Text\]](#) [\[PDF\]](#)

**Neural representation of object approach in a decision-making motor circuit.**

T. Preuss, P. E. Osei-Bonsu, S. A. Weiss, C. Wang and D. S. Faber  
*J. Neurosci.*, March 29, 2006; 26 (13): 3454-3464.

[\[Abstract\]](#) [\[Full Text\]](#) [\[PDF\]](#)

**Responses of a Looming-Sensitive Neuron to Compound and Paired Object Approaches**

B. B. Guest and J. R. Gray  
*J Neurophysiol*, March 1, 2006; 95 (3): 1428-1441.

[\[Abstract\]](#) [\[Full Text\]](#) [\[PDF\]](#)

Updated information and services including high-resolution figures, can be found at:

<http://jn.physiology.org/cgi/content/full/94/3/2150>

Additional material and information about *Journal of Neurophysiology* can be found at:

<http://www.the-aps.org/publications/jn>

---

This information is current as of March 5, 2007 .

## Time-Dependent Activation of Feed-Forward Inhibition in a Looming-Sensitive Neuron

Fabrizio Gabbiani,<sup>1,2</sup> Ivan Cohen,<sup>1</sup> and Gilles Laurent<sup>3</sup>

<sup>1</sup>Department of Neuroscience, Baylor College of Medicine, Houston, Texas; <sup>2</sup>Computational and Applied Mathematics, Rice University, Houston, Texas; and <sup>3</sup>Division of Biology, California Institute of Technology, Pasadena, California

Submitted 21 April 2005; accepted in final form 28 May 2005

**Gabbiani, Fabrizio, Ivan Cohen, and Gilles Laurent.** Time-dependent activation of feed-forward inhibition in a looming-sensitive neuron. *J Neurophysiol* 94: 2150–2161, 2005. First published May 31, 2005; 10.1152/jn.00411.2005. The lobula giant movement detector (LGMD) is an identified neuron in the locust visual system that responds preferentially to objects approaching on a collision course with the animal. For such looming stimuli, the LGMD firing rate gradually increases, peaks, and decays toward the end of approach. The LGMD receives both excitatory and feed-forward inhibitory inputs on distinct branches of its dendritic tree, but little is known about the contribution of feed-forward inhibition to its response properties. We used picrotoxin, a chloride channel blocker, to selectively block feed-forward inhibition to the LGMD. We then computed differences in firing rate and membrane potential between control and picrotoxin conditions to study the activation of feed-forward inhibition. For looming stimuli, a significant activation of inhibition was observed early, as objects exceeded on average  $\sim 23^\circ$  in angular extent at the retina. Inhibition then increased in parallel with excitation over the remainder of approach trials. Experiments in which the final angular size of the approaching objects was systematically varied revealed that the relative activation of excitation and inhibition remains well balanced over most of the course of looming trials. Feed-forward inhibition actively contributed to the termination of the response to approaching objects and was particularly effective for large or slowly moving objects. Suddenly appearing and receding objects activated excitation and feed-forward inhibition nearly simultaneously, in contrast to looming stimuli. Under these conditions, the activation of excitation and feed-forward inhibition was weaker than for approaching objects, suggesting that both are preferentially tuned to approaching objects. These results support a phenomenological model of multiplication within the LGMD and provide new constraints for biophysical models of its responses to looming and receding stimuli.

### INTRODUCTION

Feed-forward inhibition is ubiquitous in neuronal microcircuits (Shepherd 2003). Its role in synaptic integration is likely to vary across different cell types. In the hippocampus and cerebellar cortex, *in vitro* experiments suggest that feed-forward inhibition enhances coincidence detection in CA1 pyramidal cells and Purkinje cells (Mittmann et al. 2005; Pouille and Scanziani 2001). In cat visual cortex, whole cell patch recordings *in vivo* have revealed an important role of inhibition in shaping the receptive field properties of simple and complex cells (Anderson et al. 2000; Borg-Graham et al. 1998; Hirsch et al. 1998). For such directionally selective cells, inhibition is activated by motion in the preferred direction in parallel with

excitation and can sometimes result in a two- to threefold increase in membrane conductance (Monier et al. 2003). This in turn will lead to complex changes in the biophysical integration of synaptic inputs (Chance et al. 2002; Holt and Koch 1997; Kuhn et al. 2004).

Little is known about the role of feed-forward inhibition in shaping the receptive field properties of neurons sensitive to approaching objects (looming stimuli). Such neurons have been described in the visual system of several species, including monkeys, pigeons, and insects (Cooke and Graziano 2004; Fogassi et al. 1996; Gabbiani et al. 2004; Sun and Frost 1998; Wickelmaier and Strausfeld 2000). In the locust, one such identified, looming-sensitive neuron is the lobula giant movement detector (LGMD) (O'Shea and Williams 1974). Its postsynaptic target, the descending contralateral movement detector (DCMD) neuron (Gabbiani et al. 2004; Rind and Simmons 1992; Schlotterer 1977) spikes in 1:1 correspondence with the LGMD and provides a convenient way of monitoring the LGMD output activity (Fig. 1A). The LGMD receives excitatory synaptic inputs sensitive to local motion onto a large dendritic fan (labeled A in Fig. 1A) (Krapp and Gabbiani 2005; O'Shea and Williams 1974; Rowell 1971). This excitatory input is affected by several inhibitory processes (Rowell and O'Shea 1976; Rowell et al. 1977) and in particular by a phasic lateral inhibitory network effectively activated by translating and looming stimuli (Fig. 1A) (Gabbiani et al. 2002; O'Shea and Rowell 1975). In addition, the LGMD receives direct feed-forward inhibition onto two separate dendritic subfields (labeled B and C in Fig. 1A) (O'Shea and Williams 1974; Rowell et al. 1977). This inhibition is most sensitive to large, transient changes in luminance (O'Shea and Rowell 1975), with one subfield receiving inhibition in response to increases and the other subfield to decreases in luminance (separate ON and OFF channels onto subfields B and C, respectively) (Rowell et al. 1977). Except for opposite contrast sensitivities, both types of feed-forward inhibition exhibit similar response properties on visual stimulation, including temporal activation kinetics and amplitudes at high contrasts (Rowell et al. 1977). The anatomical basis for the OFF-type inhibition is best understood: it is mediated by a bundle of  $\sim 500$  axons originating from neurons whose cell bodies are located at the level of the second optic chiasm in the optic lobe (Elphick et al. 1996). Their receptive fields are thought to span  $\sim 8 \times 12^\circ$  (Rowell et al. 1977; Strausfeld and Naessel 1981).

Address for reprint requests and other correspondence: F. Gabbiani, Dept. of Neuroscience, Baylor College of Medicine, One Baylor Plaza, Houston, TX 77030 (E-mail: gabbiani@bcm.tmc.edu).

The costs of publication of this article were defrayed in part by the payment of page charges. The article must therefore be hereby marked "advertisement" in accordance with 18 U.S.C. Section 1734 solely to indicate this fact.

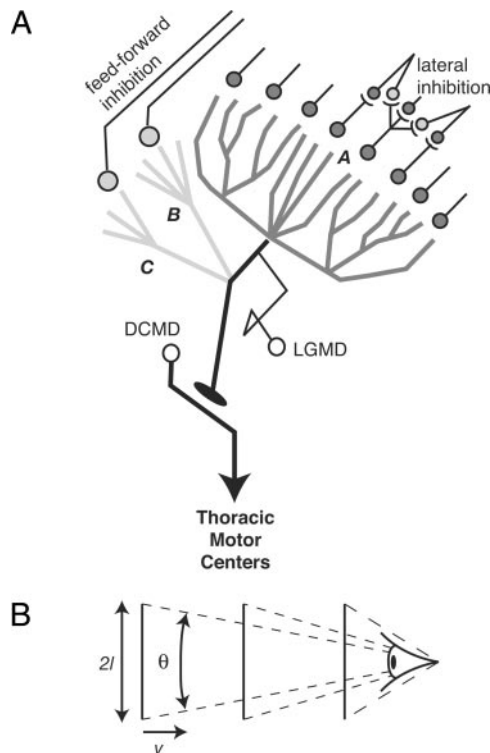


FIG. 1. Schematics of neuronal circuitry and stimulation configuration. *A*: lobula giant movement detector (LGMD) receives excitatory synaptic inputs (circles shaded in dark gray) on a large dendritic field (*A*). An important characteristic of this pathway is the presence of a lateral inhibitory network between excitatory afferent fibers presynaptic to the LGMD (inhibitory synapses are illustrated by circles shaded in light gray). ON and OFF feed-forward inhibition impinges on 2 separate dendritic fields (*B* and *C*, respectively). *B*: looming stimuli consisted of black squares on a bright background approaching at a constant speed  $v$  with half-size  $l$ . The angle subtended by the object at the retina is denoted by  $\theta$ .

Feed-forward inhibition is also activated by small field visual stimuli (Rowell et al. 1977), but its temporal pattern of activation in response to approaching objects is not well characterized. One biophysical model of the LGMD responses to looming stimuli assumed that activation occurs only immediately prior to collision, as the object covers most of one visual hemisphere, i.e.,  $\sim 180^\circ$  in angular extent (denoted by  $\theta$  in Fig. 1*B*) (Rind and Bramwell 1996). A second, phenomenological, model suggests that activation of feed-forward inhibition occurs considerably earlier and contributes to terminating the responses to looming stimuli (Gabbiani et al. 1999, 2002; Hatsopoulos et al. 1995). To characterize experimentally the time course of activation of feed-forward inhibition during object approach, we took advantage of the fact that the synapses made by afferent fibers onto the excitatory dendritic fan of the LGMD, as well as the lateral, presumed inhibitory, connections between these afferents in the lobula, are cholinergic (Rind and Simmons 1998). Thus local ejection onto the dorsal lobula of picrotoxin, a blocker of fast GABA<sub>A</sub>-mediated synaptic transmission (Rauh et al. 1990; Warzecha et al. 1993), will affect only feed-forward inhibitory inputs to subfields *B* and *C* of the LGMD. Comparing the responses of the LGMD before and after picrotoxin ejection to approaching objects as well as to other types of stimuli allowed us to characterize the temporal activation dynamics of feed-forward

inhibition relative to that of excitation. Some of our results have been briefly reported earlier (Gabbiani et al. 2002).

## METHODS

The preparation, electrophysiology, picrotoxin application, and visual stimuli were similar to those described in earlier publications (Gabbiani et al. 1999, 2001, 2002 and supplementary material<sup>1</sup>).

### Preparation

Experiments were done on adult locusts (mostly female) taken from the laboratory colony 3–4 wk after their final molt. Animals were mounted dorsal side up on a custom-designed polycarbonate holder that allowed us to reproducibly align the stimulated eye with the stimulation apparatus. For extracellular DCMD recordings, an opening was made in the pronotum, the gut was removed, and the connectives were exposed. A hook electrode consisting of two stainless steel wires 50  $\mu\text{m}$  in diameter isolated except on the recording surface was positioned under the connective contralateral to the stimulated eye using a micromanipulator. The two wires were further isolated electrically with vacuum grease, and the preparation was kept moist using locust saline. For intracellular LGMD recordings and picrotoxin-application experiments, the entire head (except for the stimulated eye) was bathed in locust saline. The head capsule was opened dorsofrontally between the two eyes. Fatty tissue overlying the brain was removed and the muscles in the head capsule were sectioned. The exposed brain was de-sheathed with fine forceps. Protease (type XIV, Sigma-Aldrich, St. Louis, MO) was sometimes used to soften the brain's protective sheath. A holder supported the brain during intracellular recordings to minimize movement.

### Electrophysiology and data acquisition

Extracellular recordings from hook electrodes were amplified differentially 10,000 times using standard equipment (A-M Systems 1700, Carlsborg, WA; Brownlee 440, San Jose, CA). Intracellular recordings were obtained with sharp microelectrodes fabricated using a horizontal puller (P-97, Sutter Instruments, Novato, CA) from thick- or thin-wall borosilicate glass (1.2/0.68 or 1.2/0.9 mm OD/ID, WPI, Sarasota, FL). They were filled with a 2 M potassium acetate aqueous solution (DC resistance: 30–70 M $\Omega$ ). The tip of the electrodes was usually dipped in black ink to facilitate visualization. After penetration, the LGMD was identified through its spikes that are in 1:1 correspondence with those of the DCMD in the connective (Fig. 2*A*). Intracellular recordings typically lasted between 40 and 60 min. Small hyperpolarizing currents (–0.5 to –1 nA) were used as needed to stabilize the recordings and did not alter the experimental results. The membrane potential with respect to the ground electrode placed in the bath solution was amplified 10 times with an Axoclamp 2B (Axon Instruments, Union City, CA). Extracellular multielectrode recordings from the medulla were obtained using silicon probes fabricated by the Center for Neural Communication Technology of the University of Michigan ('Michigan probes'). Each probe consisted of 16 recording pads arranged in tetrode configuration as illustrated in Fig. 2*A* of Pouzat et al. (2002). The recordings were amplified with a custom amplifier. All data were acquired at 12- to 14-bit resolution using A/D cards (Win30 or Powerdac series, United Electronics Industries, Canton, MA) controlled from a personal computer running the QNX operating system (QNX Software Systems, Ottawa, Canada). Intracellular recordings were sampled at 20 kHz, extracellular hook electrode recordings at 10 kHz, and extracellular Michigan probe recordings at 20 kHz.

<sup>1</sup>The Supplementary Material for this article is available online at <http://jn.physiology.org/cgi/content/full/00411.2005/DC1>.

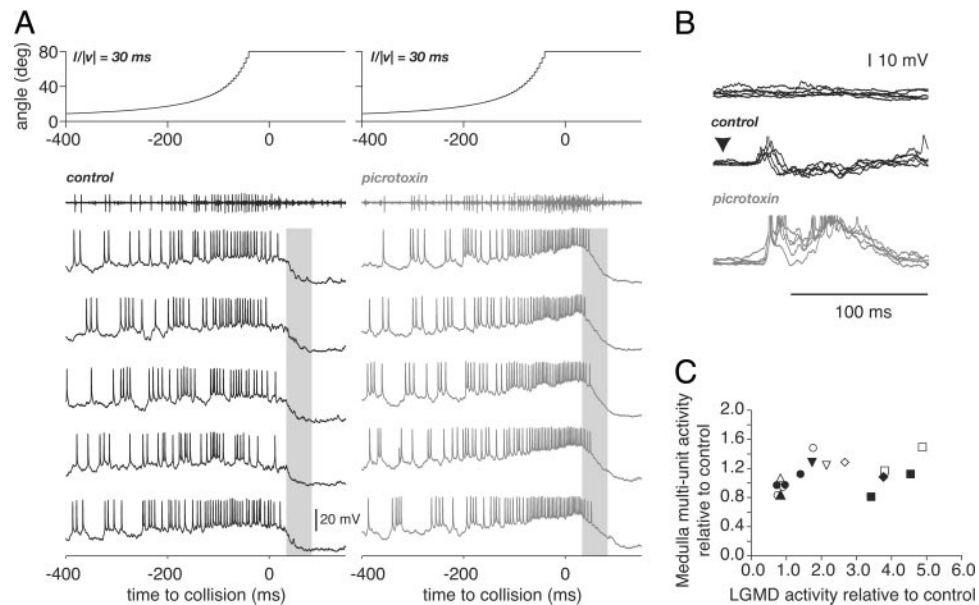


FIG. 2. Effect of picrotoxin on the responses to visual stimuli of the LGMD and of neuronal populations recorded in the medulla. *A*: 5 sample traces of intracellular recordings from the LGMD in response to a looming stimulus ( $l/|v| = 30$  ms, illustrated in the *top panels*) are shown at the *bottom*. The recordings on the *left* and *right* were obtained before and after focal pressure ejection of picrotoxin on the dorsal lobula, respectively. The 2 *extracellular traces* above the *top 2 intracellular recordings* were acquired simultaneously from the contralateral connective. The large extracellular spikes, in 1-to-1 correspondence with those of the LGMD, are from the descending contralateral movement detector (DCMD). The light gray shaded area marks the time of abrupt decrease of the LGMD membrane potential and is reproduced in *B*. *B*: intracellular recording from the LGMD in response to a fast flow stimulus activated at the time marked by the arrowhead (duration 50 ms). *Top*: membrane potential responses when the screen remained at its background luminance level. *Middle*: in the control condition, the stimulus elicits brief excitatory postsynaptic potentials (EPSPs) followed by long-lasting inhibitory postsynaptic potentials (IPSPs). *Bottom*: after focal ejection of picrotoxin on the dorsal lobula, strong excitation is unmasked (spikes are truncated). Each stimulus was presented 10 times; only 5 trials are depicted for clarity. *C*: comparison of activity increase in the LGMD (abscissa) and in neuronal populations of the medulla (ordinate) induced by focal pressure ejection of picrotoxin on the dorsal lobula. Activity increase was assessed by averaging the response to 30 consecutive looming stimuli ( $l/|v| = 25$  ms), spaced by 40–60 s, in control condition and after picrotoxin ejection. Experiments were repeated on 5 locusts, each represented as a distinct symbol shape. Activity levels were estimated either as maximum firing frequency over the looming stimulus (open symbols) or as the total number of spikes (filled symbols) and normalized to control levels. In some experiments, activity was measured after successive ejections of picrotoxin. Activity in control conditions: LGMD,  $18 \pm 10$  (SD) spikes/trial,  $57 \pm 25$  spikes/s at peak; medulla population,  $266 \pm 127$  spikes/trial,  $152 \pm 85$  spikes/s at peak. Activity after picrotoxin ejection: LGMD,  $32 \pm 7$  spikes/trial,  $116 \pm 37$  spikes/s at peak; medulla population,  $301 \pm 188$  spikes/trial,  $193 \pm 106$  spikes/s at peak.

### Picrotoxin application

Pipettes for picrotoxin ejection were pulled and fire-polished to a final diameter of  $\sim 1$   $\mu$ m using a microforge (Narishige, Tokyo, Japan). They were backfilled with picrotoxin (5 mM; Sigma) in aqueous solution containing 0.5% (wt/vol) of Fast green (Sigma) to allow visualization of the ejected liquid and to confirm visually the area affected by the ejection. The solution was heated to 35°C and stirred prior to each experiment. The pipettes were connected to a pneumatic picopump (WPI), and the ejection pressure was calibrated prior to each experiment by measuring ejected volumes in mineral oil. The ejected quantities ranged from 2 to 20 nl. During an experiment, the pipette was rapidly lowered with a micromanipulator toward the targeted site and retracted immediately after the ejection to minimize diffusion in the bath. During extracellular recordings the ejection pipette was placed in physical contact with the dorsal lobula, whereas during intracellular recordings, it was placed as close as possible to the dorsal lobula ( $\sim 20$   $\mu$ m). This procedure allowed direct application of the drug to the neuropil because the optic lobe had been previously desheated (see *Preparation*).

### Visual stimulation

A video monitor controlled by a personal computer running the QNX operating system was used to generate the visual stimuli using a commercially available graphics library (MGL, Scitechsoft, Chico, CA). The monitor was refreshed at 200 frames/s, and a synchronization pulse was issued for each frame refresh on the parallel port of the computer and acquired simultaneously with the electrophysiological

data. During an experiment, the animal's longitudinal axis was placed parallel to the screen at a distance of 15.8 cm. The center of one eye was aligned with the center of the screen. Under these conditions, the angle subtended by a screen pixel ( $0.22^\circ$ ) was well below the acceptance angle of a single ommatidium ( $\sim 1.5^\circ$ ) (Wilson 1975). The approach of black squares (half-size  $l$ , constant speed  $v$ ;  $\sim 0$   $\text{cd/m}^2$ ; Fig. 1*B*) on a white background ( $\sim 90$   $\text{cd/m}^2$ ) was simulated by perspective projection as described in Gabbiani et al. (1999). The initial size of the objects on the screen was 1 pixel, and the center of expansion of these looming stimuli coincided with the center of the screen. The time course of the angular size,  $\theta(t)$ , subtended by the object at the retina during such an approach is illustrated in Fig. 2*A*, for example (*top panels*). In this figure and subsequent ones, the discrete jumps in angular size visible toward the end of approach correspond to individual video refreshes of the monitor. By convention, the origin of the time axis corresponds to the projected collision time ( $t = 0$ ,  $\theta = 180^\circ$ ), and time before collision is negative as is the speed,  $v$ , for an approaching object. The time course of approach is uniquely characterized by the ratio  $l/|v|$  (in units of ms) (Gabbiani et al. 1999). The values used ( $l/|v| = 10, 30,$  and  $50$  ms) correspond to approaches lasting 1.1, 3.4, and 5.7 s, respectively. The relation between the half-size of the object,  $l$ , its speed of approach,  $v$ , and the value of  $l/|v|$  is given in Gabbiani et al. (1999), Table 1. The responses of the LGMD/DCMD to receding objects were studied by inverting these approach sequences. In these experiments, the black square appeared abruptly on the screen and stayed stationary for 2.5 s before the recession sequence started. The onset of recession was defined as *time 0* in such experiments (Fig. 6, *A* and *B*, *top*). In other experi-

ments, we used a fast optic flow stimulus, that has been described in Gabbiani et al. (2002; and supplementary material), consisting of alternating white and gray bars (30% contrast) rapidly moving at a temporal frequency of 50 Hz. This stimulus is well suited to activate feed-forward inhibition onto the LGMD. This rapid motion stimulus lasted 50 ms and was preceded and followed by 1 s during which the screen was set to a white background.

### Experimental protocols

To facilitate reference in the Results, each protocol is numbered in the following description.

P1. In a first series of experiments, we studied the time course of the firing rate and the intracellular membrane potential of the LGMD during looming. Two looming stimuli were used with  $l/|v|$  values of 10 and 30 ms and a final approach angle of  $80^\circ$ . Each stimulus was presented pseudorandomly five times before and after picrotoxin application with an intertrial interval of 20 s. The intertrial interval during intracellular recordings was shorter than during extracellular recordings (see P3–P9 in the following text) to compensate for shorter recording times and acquire sufficient data for statistical analyses. This led to slightly increased habituation of the responses in some animals. During these experiments, two additional stimuli combining the looming and fast-flow stimuli were also presented five times before and after picrotoxin application, and the resulting data have been reported earlier (Gabbiani et al. 2002; their Fig. 3a). The experiment was performed on six animals and typically lasted between 40 and 60 min. An additional group of four animals were tested with the same visual stimulation protocol. In these experiments, just the firing rate of the LGMD was monitored extracellularly via DCMD hook electrode recordings.

P2. Next, we studied the intracellular membrane potential of the LGMD to presentation of the fast flow stimulus before and after picrotoxin ejection. Once intracellular recordings from the LGMD were obtained and confirmed by paired hook electrode recordings of the DCMD, 10 presentations of the fast-flow stimulus were alternated pseudo-randomly with 10 presentations of a white background of equal duration (inter-trial interval: 20 s; white background between trials). Another set of 20 presentations was carried out after picrotoxin ejection. The protocol was applied on four animals (duration:  $\sim 20$  min).

P3. P3 was a series of experiments aimed at estimating the effect of a possible diffusion of picrotoxin from the lobula onto medulla neurons upstream of the LGMD. Medulla multi-unit responses were recorded with the 16-channel Michigan probe while the LGMD/DCMD firing was monitored with hook electrodes placed on the contralateral connective. In these experiments, 30 looming stimuli ( $l/|v| = 25$  ms) were presented spaced by time intervals of 40–60 s, in control condition and after pressure ejection of picrotoxin on the dorsal lobula. The activity was sometimes measured after successive ejections of picrotoxin. This protocol was carried out on five locusts (duration:  $\sim 1.25$  h).

P4. In the next set of experiments, the time course of the LGMD/DCMD firing rate was monitored extracellularly while presenting looming stimuli at three different  $l/|v|$  values (10, 30, and 50 ms). The approach sequence stopped at one out of four final angular sizes: 20, 40, 60, or  $80^\circ$ . Each of the 12 possible stimuli ( $3 l/|v|$  values  $\times 4$  final sizes) was presented eight times in pseudorandom order with an intertrial interval of 40 s. This protocol lasted  $\sim 1.25$  h and was applied to 14 animals. To assess a possible effect of habituation on the responses (Rowell 1974), the same protocol was applied to an additional set of six animals with a longer intertrial interval (160 s) and a decreased number of trials (2 per stimulus) to keep the duration of the experiment approximately unchanged.

P5. A similar protocol was used to study the effect of picrotoxin on the LGMD/DCMD responses during looming. In these experiments, the approaches with the two smallest final angular sizes ( $20$  and  $40^\circ$ ) were presented first at three  $l/|v|$  values (10, 30, or 50 ms) selected pseudorandomly, followed by the two largest final angular sizes ( $60$  and  $80^\circ$ ; same  $l/|v|$  values selected pseudorandomly). Each of these 12 stimuli ( $3 l/|v|$  values  $\times 4$  final sizes) was presented three times with a 60-s intertrial interval both before and after picrotoxin application (experiment duration:  $\sim 1.5$  h). The protocol was applied to 10 animals.

P6. To study quantitatively the effect of picrotoxin on looming responses obtained with different final approach angles, we performed experiments similar to those described under P5, but at a fixed value of  $l/|v|$ . The four final angles ( $20$ ,  $40$ ,  $60$ , and  $80^\circ$ ) were presented pseudorandomly, and the number of stimulus presentations was increased to 10 by applying intertrial intervals of 60 s. The same stimuli were presented after picrotoxin application (experiment duration:  $\sim 1.5$  h). We tested five animals at  $l/|v| = 10$  ms, five additional animals at  $l/|v| = 30$  ms, and five others at  $l/|v| = 50$  ms.

P7. To investigate the effect of picrotoxin on the LGMD/DCMD responses to receding stimuli, we started by using four initial angles ( $20$ ,  $40$ ,  $60$ , and  $80^\circ$ ) and three  $l/|v|$  values (10, 30, and 50 ms). Each of these 12 stimuli was presented three times pseudorandomly before and after picrotoxin application at intertrial intervals of 60 s. This experiment was performed on five animals and lasted  $\sim 1.25$  h.

P8. Next, we performed experiments at a single  $l/|v|$  value (30 ms) and four start angles ( $20$ ,  $40$ ,  $60$ , and  $80^\circ$ ) to study quantitatively the effect of picrotoxin on the responses to receding objects. This allowed us to present each stimulus eight times pseudorandomly for a similar experiment duration as in protocol 7 (intertrial interval: 60 s). This protocol was used on five animals.

P9. Finally, we studied the effect of picrotoxin on the responses to receding objects at three  $l/|v|$  values (10, 30, and 50 ms) for a single initial angle of  $40^\circ$ . Each stimulus was presented pseudorandomly 10 times (60-s intertrial interval; duration of experiment:  $\sim 1.25$  h). This protocol was applied on five animals.

### Data analysis

During data analysis, we routinely screened for possible habituation of the LGMD/DCMD responses. LGMD/DCMD spikes were extracted from the extra- or intracellular potential traces by thresholding (Gabbiani et al. 1999). Estimates of the instantaneous firing rate were then obtained by convolution of the resulting spike trains with a Gaussian kernel ( $\sigma = 20$  ms). The time shifts introduced during convolution by the discrete Fourier transform were compensated for. The resulting spike density function was normalized to yield the total number of spikes after integration over the duration of the trial. For the experiments of P3, extracellular spike time detection was performed as described in Cohen and Miles (2000) using routines written in the LabVIEW programming environment (National Instruments, Austin, TX; available at <http://glab.bcm.tmc.edu/Spikoscope>). Multi-unit activity was quantified by counting the total number of spikes during a trial pooled across the 16 recording sites of the Michigan probe. In addition, estimates of peak multiunit instantaneous firing frequency were obtained after convolution of the pooled spike trains with a Gaussian kernel as described in the preceding text ( $\sigma = 50$  ms). Both the total number of spikes and peak firing rates were averaged over 30 consecutive looming trials.

The time course of the subthreshold membrane potential during looming was obtained from the intracellular membrane potential of the LGMD (P1) by median filtering (15-ms sliding window). To facilitate comparison with the time course of the instantaneous firing rate, the resulting traces were subsequently convolved with a Gaussian

filter ( $\sigma = 20$  ms). Differences in the mean instantaneous firing rate or the time course of the subthreshold membrane potential (Fig. 3) were assessed by a *t*-test taking into account unequal variances (Smith-Satterthwaite method) (Milton and Arnold 1995).

During the presentation of a looming stimulus, the response of the LGMD/DCMD typically increases, peaks, and decays to spontaneous levels at the end of stimulation (Fig. 4) (Gabbiani et al. 1999, 2001, 2002; Matheson et al. 2004). When analyzing the data obtained with protocols 4–6, we quantified the time at which the responses of the LGMD/DCMD to looming stimuli stopped using two different methods. In the first method, we computed the time at which the instantaneous firing decayed to 20% of its mean peak value (Fig. 4,  $\blacktriangle$ ). In the second method, we computed for each trial the time at which the last spike occurred, excluding those spikes occurring after the mean instantaneous firing rate had decayed to <15% of its peak value. This 15% criterion allowed to exclude outliers occurring well after the end of stimulation, such as those marked in Fig. 4A ( $\blacklozenge$ , right panel in 1st row). The last spikes computed by this method are marked by a leftward pointing arrowhead ( $\blacktriangleleft$ ) for each spike raster in Figs. 4 and 5.

All data analysis was performed using Matlab (Mathworks, Natick, MA). The measures of variability illustrated in all the figures are SDs. In Figs. 4–7, spike rasters are arranged in ascending chronological order: for each stimulus, the first presentation corresponds to the bottom raster and the last one to the top raster. Because stimuli were chosen pseudorandomly, the time interval between two successive presentations of the same stimulus is variable. The nonparametrical statistical tests used in RESULTS are described in Lehmann (1998). The analysis of covariance applied to P4–P6 is described in Mickey et al. (2004).

## RESULTS

This report is based on recordings performed on 79 different animals. Data collected in 14 of those animals has been briefly reported earlier (Gabbiani et al. 2002).

### *Block of feed-forward inhibition onto the LGMD by picrotoxin*

Both the LGMD and its postsynaptic target, the DCMD, respond vigorously to objects approaching on a collision course with the animal. This is illustrated in Fig. 2A, where the top panel depicts the angle subtended at the retina by an approaching black square. The half-size to speed ratio of the square was  $l/|v| = 30$  ms (Fig. 1B,  $l =$  half-size,  $|v| =$  approach speed; METHODS, P1). The bottom five intracellular traces are successive recordings from a single LGMD neuron in response to this looming stimulus. The top extracellular trace is a simultaneous recording of the DCMD activity in 1:1 correspondence with the top intracellular trace. In this example, the LGMD/DCMD response increased gradually during the approach sequence and stopped  $\sim 50$  ms after the last frame of object motion. The LGMD receives both excitation and feed-forward inhibition onto its dendritic tree. Thus the termination of the response may be due to activation of feed-forward inhibition or termination of excitation or a combination of both. An active role of feed-forward inhibition may be inferred from the steep decrease in membrane potential (Fig. 2A, shaded area) after the last LGMD spikes, suggesting that IPSPs contribute to terminate the response. To address this question more directly, we ejected picrotoxin, a blocker of GABA<sub>A</sub> channels, locally onto the dorsal lobula where the LGMD receives its inhibitory inputs (Rowell et al. 1977; Strausfeld and Naessel 1981). The effect of picrotoxin was noticeable almost immediately,

i.e., within a few minutes of application. It lasted over the entire duration of an experiment, for typically as long as 45 min (see *Experimental protocols*). Figure 2A, right, illustrates the responses obtained in the same neuron after picrotoxin application. The number of spikes elicited over the course of looming was considerably increased (on average from 49 to 78,  $n = 5$  trials) as was the duration of the response with the time of the last spike occurring on average 36 ms later in picrotoxin (last spike times in control and picrotoxin were on average 11 and 47 ms after collision, respectively). Furthermore, the decay of the membrane potential after picrotoxin application was less rapid than it was in controls (compare the membrane potential time course in Fig. 2A, shaded areas). These observations repeated in a total of six animals suggest a role of feed-forward inhibition in terminating the response to object approach (Rind 1996).

To verify that picrotoxin was acting postsynaptically on feed-forward inhibition onto the LGMD, we performed a series of experiments using a visual stimulus consisting of alternating white and gray stripes rapidly translating across the visual field (fast optic flow stimulus; METHODS, P2). Similar stimuli have been reported earlier to effectively activate feed-forward inhibition (O'Shea and Rowell 1975; Rowell et al. 1977). Figure 2B, top two panels, confirms this observation: when the fast optic flow stimulus was presented (middle, arrowhead), an EPSP was elicited, rapidly followed by a strong IPSP recorded after a latency of  $\sim 40$  ms and lasting  $\sim 100$  ms. In contrast, background illumination did not elicit any detectable responses (Fig. 2B, top). After picrotoxin ejection, the fast flow stimulus elicited strong excitation in the LGMD (Fig. 2B, bottom), consistent with a block of GABAergic inhibition and suggesting that the fast flow stimulus is also effective at activating excitation onto the LGMD. Under control conditions, however, this excitation appears to be tightly controlled by feed-forward inhibition.

In addition to its effect on the LGMD, ejection of picrotoxin onto the dorsal lobula may also affect the activity of presynaptic neurons in the medulla or lamina. This appears unlikely as these two neuropils are located several hundreds of micrometers away from the lobula. Nonetheless, to directly address this possibility, we performed extracellular multielectrode recordings in the medulla while monitoring simultaneously the activity of the LGMD/DCMD during looming (METHODS, P3). The multielectrode probes were placed  $\sim 200$   $\mu$ m distal to the lobula and sampled a region where retinotopic motion-sensitive units are routinely recorded (Cohen and Gabbiani 2003). The mean number of spikes and the mean peak firing rate elicited by the looming stimulus were computed for both the recorded medulla neuron populations and the LGMD. Values obtained after picrotoxin ejection were expressed relative to control levels, prior to picrotoxin ejection. Figure 2C shows the mean peak firing rates and numbers of spikes (open and filled symbols, respectively) after picrotoxin application relative to control for medullary neuron populations as a function of those recorded in the LGMD. There was little increase in medullary population activity under picrotoxin (average of 3 and 19% above control for spike counts and peak firing rates,  $n = 5$  animals) compared with that observed in the LGMD (average of 118 and 125% above control), suggesting that the effect of picrotoxin was localized and predominantly postsynaptic. The magnitude of LGMD mean and peak firing

rate changes after picrotoxin application was variable across experiments. Despite this variability, the resulting changes in the characteristics of the responses described in the following were consistent across animals.

### Time-dependent activation of feedforward inhibition during looming

The data illustrated in Fig. 2A show that the firing rate of the LGMD is considerably higher in picrotoxin than in control conditions over a large fraction of the looming approach. This suggests a substantial role of feed-forward inhibition in controlling excitation before the termination of the response, in the time window that corresponds to the shaded area in Fig. 2A. Thus in control conditions, excitation appears to mask a concurrent activation of inhibition. To investigate quantitatively the time course of activation of feed-forward inhibition during looming, we computed from the data obtained from P1 an estimate of the instantaneous firing rate of the LGMD/DCMD before and after picrotoxin ejection. Figure 3A (*middle*) illustrates these instantaneous firing rates for the same neuron as in Fig. 2. The difference between the two traces and its 95% confidence interval are illustrated in the *bottom panel* (black line and dark gray surrounding area, respectively). This difference between control and picrotoxin conditions is a measure of the activation of feed-forward inhibition during looming independent of how excitation and feed-forward inhibition interact within the LGMD and can be seen to gradually increase during object approach. Activation of inhibition reaches its peak after the peak in firing rate during control conditions (Fig. 3A,

*middle*, black line) and subsequently starts to decay in parallel to the instantaneous firing rate during the termination of the response (light gray shaded area) that follows the cessation of object motion. A significant activation of feed-forward inhibition was detected when the object exceeded an angular size of  $22.5^\circ$  (arrowhead and dashed lines in Fig. 3A, *bottom*). On average, this detection angle amounted to  $23.3 \pm 19^\circ$ ,  $n = 6$  animals) when pooled across the two  $l/|v|$  values tested. The range of detection angles observed at  $l/|v| = 30$  ms (mean:  $28.6 \pm 14.2^\circ$ ) was significantly larger than that observed at  $l/|v| = 10$  ms (mean:  $18.1 \pm 22.4^\circ$ ; Wilcoxon rank-sum test,  $P = 0.019$ ). Figure 3B illustrates for the same cell the mean subthreshold membrane potential before and after picrotoxin application (*middle*) and the mean and 95% confidence interval for their difference (*bottom*). The difference in membrane potentials has qualitatively the same shape as the difference in firing rates in Fig. 2A. However, the membrane potential difference was a less sensitive measure of feed-forward inhibition activation as significant differences (arrowhead,  $52.5^\circ$ ) were consistently detected later than at the level of the instantaneous firing rate (mean significant membrane potential difference for 6 animals at 2  $l/|v|$  values:  $67.6 \pm 24.3^\circ$ ). In this experiment, the peak in membrane potential difference (Fig. 3B, shaded area) coincided with the onset of response termination in control conditions (Fig. 2A). The weaker sensitivity of membrane potential differences as compared with instantaneous firing rate differences will be considered in DISCUSSION. Because we wanted to characterize the dynamical properties of feed-forward inhibition, we focused on analyzing the LGMD/DCMD firing rate rather than its membrane potential in subsequent experiments.

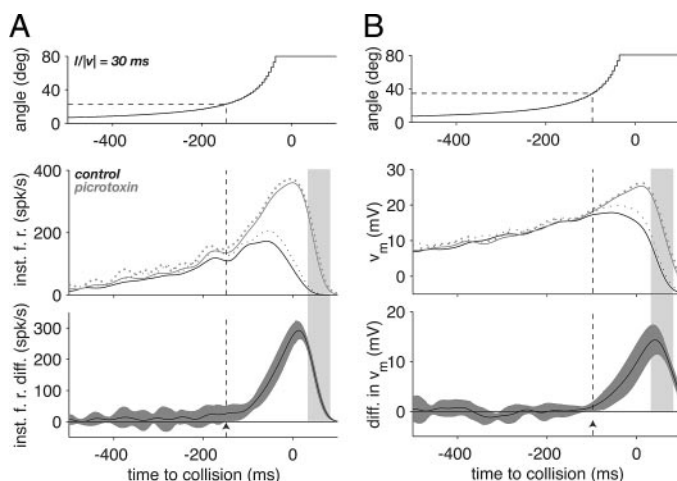


FIG. 3. Effect of picrotoxin on the time course of the LGMD instantaneous firing rate and membrane potential during a looming stimulus. *A*, *top*: the time course of the stimulus angular size as a function of time to collision. *Middle*: the time course of the firing rate (mean and mean + SD, solid and dotted lines) in control (black) and picrotoxin conditions (gray). *Bottom*: the firing rate difference between the picrotoxin and control conditions (black line) as well as its 95% confidence interval (gray). The arrowhead shows the location where the lower confidence interval boundary crosses the 0 difference line corresponding to a statistically significant change in firing rate. The time when statistical significance is reached and the corresponding angular size are given by the dashed vertical and horizontal lines, respectively. *B*: time course of the stimulus (*top*), median, low-pass filtered membrane potential (*middle*) and the difference in median, low-pass filtered membrane potential (*bottom*). Same plotting conventions as in *A*. Data illustrated in *A* and *B* correspond to the data illustrated in Fig. 1A. The light gray shaded area delimits the same time interval as in Fig. 1, *A* and *B*.

### Responses to looming stimuli of different final angles in control and picrotoxin conditions

The experiments illustrated in Figs. 2 and 3 suggest that as an object approaches, both excitation and feed-forward inhibition onto the LGMD increase in parallel. To gain further insight on their relative time course of activation, we performed experiments in which a looming stimulus stopped its approach at four different final angular sizes (20, 40, 60, or  $80^\circ$ ; METHODS, P4). According to the results presented in the preceding text, this protocol is expected to lead to increasing levels of excitation and feed-forward inhibition, correlated with the increasing final angular size of the stimulus. The dynamics of visual stimulation might also affect the relative balance of excitation and feed-forward inhibition within the LGMD. To assess this point, we used three different values of the approach parameter  $l/|v|$  (10, 30, and 50 ms). Figure 4A illustrates the data obtained in 1 of 14 experiments in which both the final angle and the kinematical parameter  $l/|v|$  were systematically varied. Qualitatively similar results were obtained in the remaining experiments and in another six animals when a longer intertrial interval was used (METHODS, P4). The *top row* illustrates the stimuli, and *each row underneath* corresponds to a different final angle. Each column corresponds to a single value of  $l/|v|$ , leading to a total of 12 possible combinations of final angles and  $l/|v|$  values. The spike rasters in each condition were used to compute estimates of the instantaneous firing rate (illustrated above the rasters) and to extract further quantitative measures of the responses. Both the

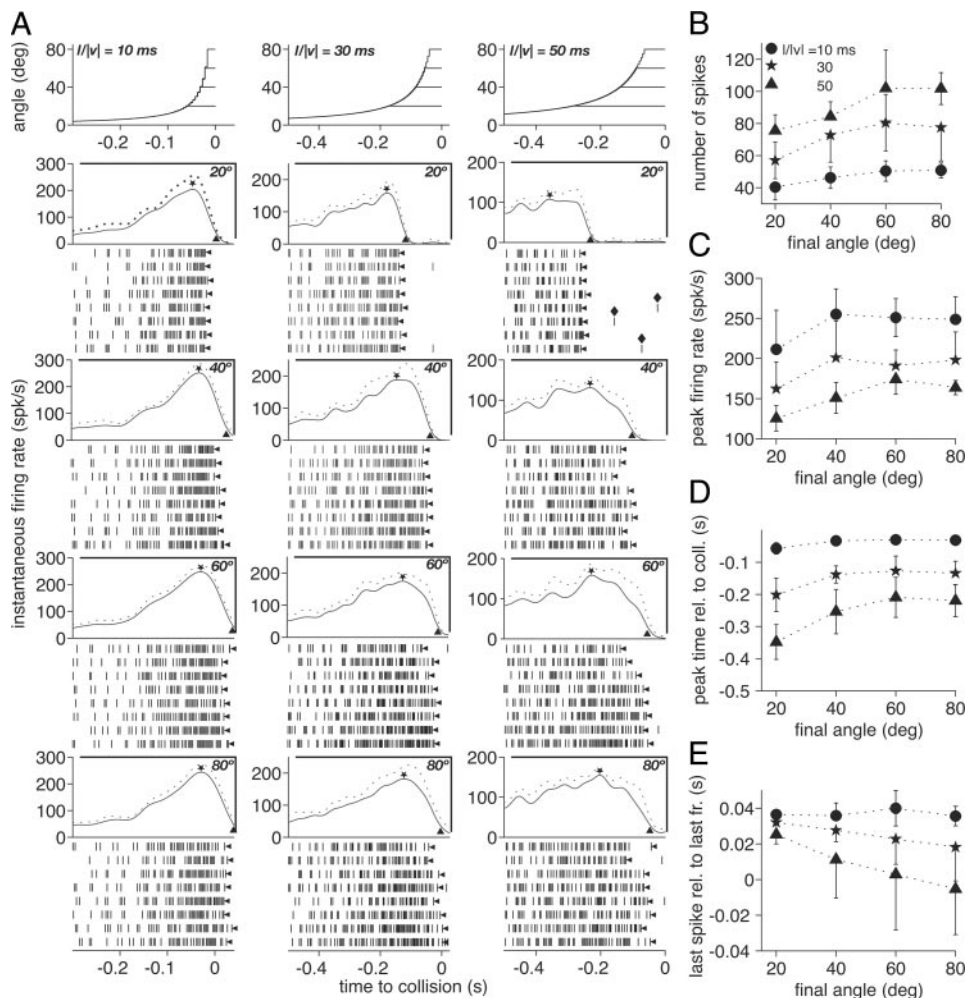


FIG. 4. Responses of the DCMD to approaching squares at 3  $l/|v|$  values and 4 final approach angles. *A*: angle subtended at the retina by the approaching square is plotted in the *top 3 panels* as a function of time to collision. Each panel corresponds to a different  $l/|v|$  value (10, 30, and 50 ms) and depicts the time course of angular size for 4 final angles (20, 40, 60, and 80°). *Four bottom panels* (below the stimuli): time course plotted of the instantaneous firing rate (mean and mean + SD, — and ···) as a function of time to collision for the 4 final angular sizes. In each panel, ★, the mean peak firing rate; ▲, the firing rate corresponding to 20% of the peak. Rasters of spikes below each panel are responses for 8 individual trials. ◀, the last spike of the trials (as defined in METHODS). ♦, spikes are examples of outliers excluded by the 15% criterion (METHODS). *B*: number of spikes (mean and SD) as a function of final angular size of the approaching square. Each symbol denotes a different  $l/|v|$  value. *C*: peak firing rate (mean and SD) as a function of final angular size. *D*: time of peak firing (mean and SD) as a function of final angular size. *E*: time of last spike (◀ in *A*; mean and SD) as a function of final angular size. The significance of symbols in *C–E* is the same as in *B*.

number of spikes (Fig. 4*B*) and the peak firing rate (Fig. 4*C*; ★ in Fig. 4*A*) increased and plateaued with final angle, irrespective of  $l/|v|$ . The increase was most pronounced from 20 to 40° [ $35 \pm 64\%$  for the number spikes and  $25 \pm 39\%$  (means  $\pm$  SD) for the peak firing rate; average across 14 animals for 3  $l/|v|$  values]. Both variables remained relatively stable thereafter and over the same sample, there was only a  $7 \pm 26\%$  increase in mean spike number from 40 to 80° and on average no increase in peak firing rate (SD: 16%). Figure 4*D* illustrates the timing of the peak firing rate relative to collision. Consistent with the previous observations, the peak occurred closer to collision as angular size increased from 20 to 40° ( $34 \pm 12\%$  decrease on average over 14 animals for 3  $l/|v|$  values), but there was much less change beyond a final angular size of 40° (on average a  $10 \pm 29\%$  decrease from 40 to 80°). These results suggest that, once activated, feed-forward inhibition rapidly controls the level of excitation. This control of excitation proceeds independent of time or of the stimulus dynamics up to the peak firing rate.

Next, we investigated two measures of the termination of the response: the time at which the mean instantaneous firing rate decreased to 20% of its peak value (▲ in the instantaneous firing rate plots of Fig. 4*A*; see *Data analysis*) and the time of the last spike evoked by the stimulus (Fig. 4*A*, ◀), excluding potential outliers (see *Data analysis*). Both measures yielded similar results, and only the second one will be illustrated.

Figure 4*E* shows the time of the last spike relative to the last frame of stimulus motion as a function of the final angular size of the stimulus for the three  $l/|v|$  values. At 20° the last spike occurred  $\sim 30$  ms after the last frame of stimulation, independent of  $l/|v|$ . For  $l/|v| = 10$  ms, this value changed little with final angle. However, the last spike occurred increasingly earlier as the final angle increased for  $l/|v| = 30$  ms, and this trend was most pronounced for  $l/|v| = 50$  ms. When fitted separately with straight lines, the slopes for the three  $l/|v|$  values were significantly different [analysis of covariance,  $F(2,90) = 4.48$ ,  $P = 0.014$ ]. These results suggest that as final angular size and, consequently, feed-forward inhibition increase, the latter is able to overcome excitation sooner after peak firing occurred, particularly for slow approach sequences. To confirm this hypothesis, we compared the timing of the last spike relative to the last motion frame before and after picrotoxin application. Figure 5*A* illustrates the spike rasters and instantaneous firing rates obtained in such an experiment where  $l/|v|$  was fixed at 30 ms (METHODS, P6). The time of the last spike relative to the last motion frame before and after picrotoxin application is illustrated in Fig. 5*B*, *top*. Its value decreased with increasing final angle in control conditions, a tendency that was abolished by picrotoxin application. Figure 5*B*, *middle*, illustrates the outcome of a similar experiment for which the value of  $l/|v|$  was set to 50 ms. In control conditions, the change in last spike time as a function of final angle was



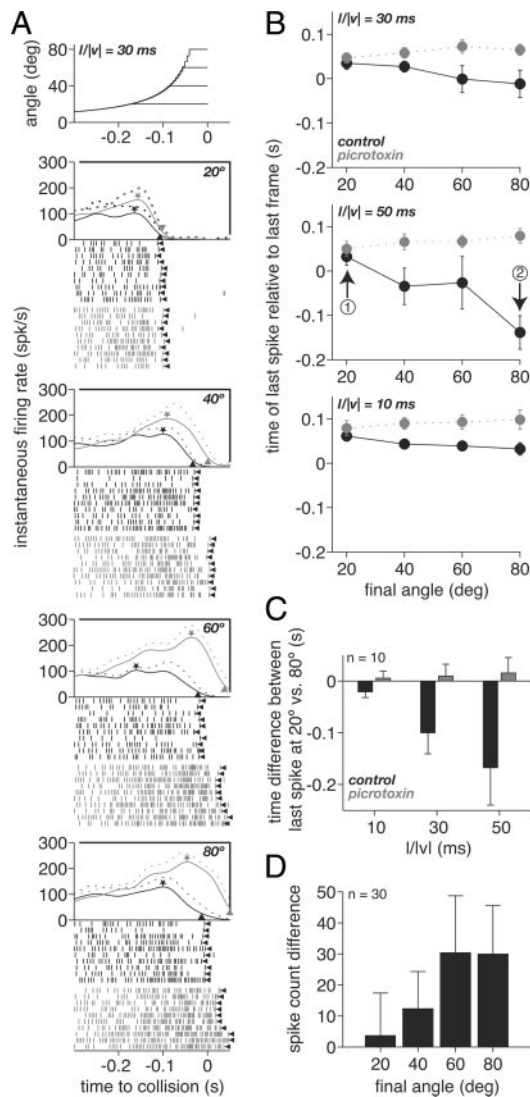


FIG. 5. Effect of picrotoxin on the responses of the DCMD to approaching squares. *A*, *top*: the angle subtended at the retina by the approaching squares is plotted as a function of time to collision. Each of the 4 curves corresponds to an approach ending with a different final angular size (20, 40, 60, and 80°) at a single  $l/|v|$  value (30 ms). *Bottom 4 panels*: the time course of the instantaneous firing rate (mean and mean + SD, solid and dotted lines) as a function of time to collision for the 4 final angular sizes before and after picrotoxin ejection (black and gray traces, respectively). In each panel, a star indicates the mean peak firing rate and a triangle points to the firing rate value corresponding to 20% of the peak. Rasters of spikes below each panel are responses for 10 individual trials before and after picrotoxin ejection (black and gray rasters, respectively). The leftward pointing arrowhead indicates the last spike of the trial (defined in METHODS). *B*: the time of last spike relative to the last frame of stimulation is plotted as a function of the final angle subtended by the stimulus at the retina before and after picrotoxin ejection (black and gray symbols). Each of the 3 panels correspond to squares approaching with a different  $l/|v|$  value (10, 30, and 50 ms) obtained in 3 different experiments (*top panel* is derived from data in *A*). The arrows labeled ① and ② in the *middle panel* point to an example of the 2 values used to derive the plot in *C*. *C*: plot of the mean time difference between the last spike relative to the last stimulus frame at a final approach angle of 20 and 80° (i.e., data point indicated by arrow ② minus that indicated by arrow ① in *B*) as a function of the approach parameter  $l/|v|$  (mean and SD across 10 experiments). Black and gray bars denote experiments before and after picrotoxin ejection, respectively. *D*: mean difference in spike counts before and after picrotoxin ejection as a function of the final angle subtended at the retina by the approaching object (mean and SD across 10 experiments and 3  $l/|v|$  values).

more pronounced than it was for  $l/|v| = 30$  ms, consistent with the data of Fig. 4*E*. After picrotoxin application, this dependence was completely abolished. Similar results are illustrated in one example for  $l/|v| = 10$  ms in Fig. 5*B*, *bottom*. The other experiments performed using this protocol (P6, METHODS) yielded similar results for all three  $l/|v|$  values. Qualitatively identical observations were also made in 10 additional experiments where the three  $l/|v|$  values were presented in the same animal at the expense of a lower number of stimulus repetitions (METHODS, P5). Figure 5*C* shows for these 10 experiments, the mean difference between the time of the last spike relative to the last frame at final angular sizes of 80 and 20° both in picrotoxin and control conditions. This corresponds to subtracting the ordinate of point ② from that of point ① in Fig. 5*B*, *middle*. In control conditions, as  $l/|v|$  increases, the difference increases, reflecting the fact that for a final size of 80°, the last spike occurs increasingly earlier relative to the last frame (e.g., Fig. 4*E*). This trend is abolished by picrotoxin application and the last spike occurs a fixed time after the last frame, irrespective of  $l/|v|$ . Figure 5*D* shows the mean difference in number of spikes in the same 10 experiments, pooled across the three  $l/|v|$  values as a function of final angular size. On average, picrotoxin application caused a mean response increase with a plateau at  $\sim 30$  spikes per trial when the final angular size exceeded 40°. The plateau observed above 40° was also obtained when analyzing each  $l/|v|$  value separately.

#### Effect of picrotoxin on LGMD/DCMD responses to receding stimuli

Next, we investigated the responses of the LGMD/DCMD to objects appearing and then receding away from the animal. In these protocols (P7–P9, METHODS), the black square suddenly appeared on the screen, stayed stationary for 2.5 s, and subsequently receded in a sequence that was reversed in time compared with that of approaching stimuli. In Fig. 6*A*, the responses to object appearance at four different angular sizes (20, 40, 60, and 80°; *top*) is illustrated for one experiment. Four additional experiments yielded similar results (P8, METHODS). As may be seen by inspection of the spike rasters elicited in control conditions (Fig. 6*A*, black), the smallest object size elicits the strongest response. Accordingly, both the mean number of spikes and the peak in firing rate were highest for an angle of 20° (Fig. 6, *A*, instantaneous firing rate plots above rasters; and *C*, *top* and *middle*, respectively, black bars). The mean number of spikes, for example, declined by 73% from 20 to 80° ( $89.2 \pm 10\%$  on average across 5 animals). This is consistent with the strength of inhibition increasing in parallel with the area of the visual field affected by the rapid change in luminance caused by the object. Interestingly, the latency of the response systematically decreased with object size in spite of the decrease in firing rate. The mean latency value observed at 20° was  $\sim 200$  ms; it was reduced to  $<100$  ms at 80° (Fig. 6*C*, *bottom*, black bars). On average, the latency decreased by  $80 \pm 69$  ms or 32% from 20 to 80° ( $n = 5$  animals). In this experiment and in four additional ones, the dependence of latency on object size was only slightly affected by block of feed-forward inhibition through picrotoxin ejection (Fig. 6, *A*, gray rasters, and *C*, *bottom*, gray bars). In contrast, both the number of spikes and the peak firing rates increased and plateaued at values independent of object size after picrotoxin

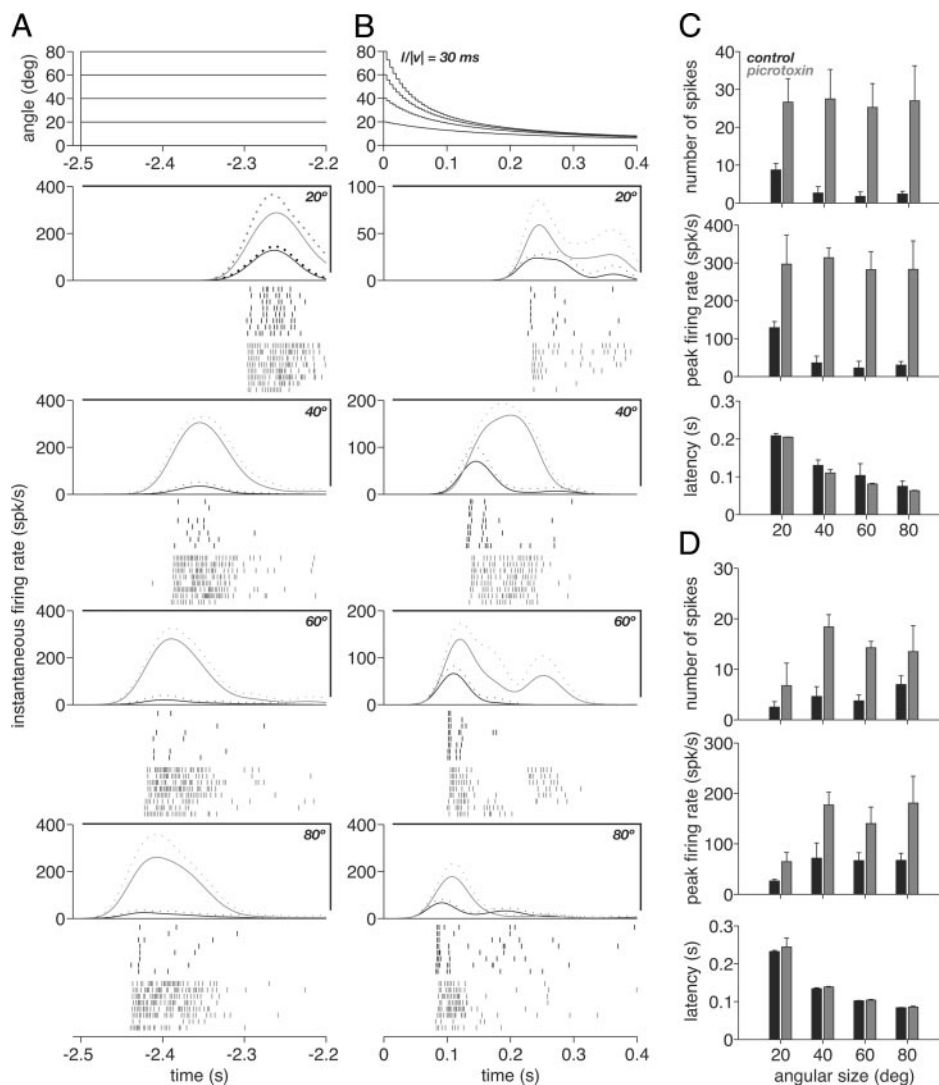


FIG. 6. Responses of the DCMD to the appearance and recession of a black square before and after picrotoxin ejection. *A*, top: the angle subtended at the retina by the appearing stimuli is plotted as a function of time. *Bottom 4 panels*: the instantaneous firing rate (mean and mean + SD, solid and dotted lines) before and after picrotoxin ejection (black and gray) is plotted separately for each angular size (20, 40, 60, and 80°). The rasters of spikes below each panel correspond to the eight trials before and after picrotoxin ejection (black and gray). *B*: the angle subtended at the retina by the receding squares is plotted as a function of time on top ( $l|v| = 30$  ms). Instantaneous firing rate and spike rasters are plotted below using the same conventions as in *A*. *C*: panels from top to bottom give summary statistics for the number of spikes, the peak firing rate, and the latency to the 1st spike after stimulus appearance, respectively (obtained from *A*). In each case, the mean over 8 trials is given as a function of the angular size of the appearing stimulus. Black and gray bars correspond to trials before and after picrotoxin ejection, respectively. Error bars denote SD. *D*: summary statistics for receding squares (obtained from *B*). Same plotting conventions as in *C*.

ejection (Fig. 6*C*, top and middle, gray bars). At a size of 20° the mean number of spikes was multiplied on average by a factor  $2.7 \pm 1.2$  and the peak firing rate by a factor  $2.4 \pm 0.7$  after picrotoxin application ( $n = 5$  animals).

Figure 6*B* shows the responses to receding objects of increasing initial size both before and after picrotoxin ejection. In control conditions, the LGMD/DCMD reproducibly fired one to two spikes after the onset of motion (see also Fig. 7*A*). A few additional spikes were also fired later during the trials. Both the mean number of spikes and the peak firing rates increased after block of feed-forward inhibition (Fig. 6, *B*, black vs. gray rasters, and *D*, top and middle). On average, at a starting size of 80° the mean number of spikes was multiplied by a factor  $3.5 \pm 1.6$  and the peak firing rate by a factor of  $3.4 \pm 1.0$  after picrotoxin application ( $n = 5$  animals). However, both in control and after picrotoxin ejection, the total number of spikes and peak firing rates elicited were smaller than those elicited by time-reversed, approach sequences (e.g., Fig. 4, *B* and *C*). This suggests both excitation and feed-forward inhibition to be less strongly activated by receding than approaching objects. The changes in latency as a function of initial angular size were very similar to those observed for abruptly appearing squares across all five animals (compare, e.g., Fig. 6, *A* and *B*). We also

performed experiments in which the start size of the receding object was fixed and the kinematical parameter  $l|v|$  was varied between 10, 30, and 50 ms (METHODS, P9). The rasters and instantaneous firing rate before and after picrotoxin ejection in such an experiment are illustrated in Fig. 7*A*. There was little dependence of the mean spike numbers, peak firing rate or response latency on the kinematical parameter  $l|v|$  (Fig. 7, *B–D*). In this particular neuron, response latency ( $\sim 50$  ms) was shorter than in the example illustrated in Fig. 6. The range of latencies to receding stimuli ranged from 54 to 235 ms (mean:  $120 \pm 63$  ms) for  $l|v| = 30$  ms and a 40° initial angle in ten animals. Similar results were obtained in an additional set of four animals tested with the same protocol and in another five animals where both  $l|v|$  and start size were varied together (P7, METHODS).

## DISCUSSION

This study investigated what effect localized picrotoxin injection to the dorsal lobula had on the responses of the LGMD/DCMD to three types of visual stimuli presented in the center of its receptive field: approaching, suddenly appearing, and receding squares. Picrotoxin had a marked effect on the

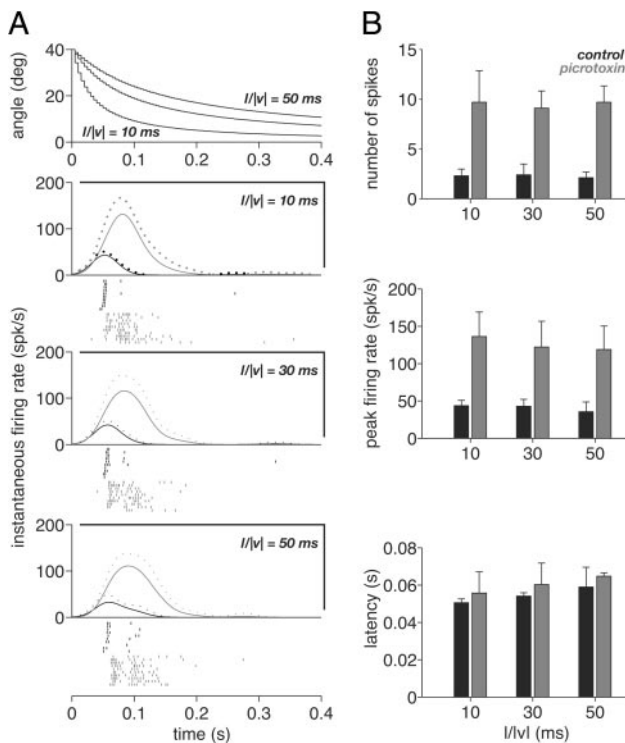


FIG. 7. Responses of the DCMD to a black square receding from a fixed initial angular size ( $40^\circ$ ) at 3 half-size to speed ratios ( $l/v| = 10, 30, \text{ and } 50 \text{ ms}$ ). *A*, *top*: the angle subtended at the retina by the receding squares is plotted as a function of time. *Bottom 3 panels*: the instantaneous firing rate (mean and mean + SD, solid and dotted lines) before and after picrotoxin ejection (black and gray). Spike rasters below each panel correspond to the 10 trials before and after picrotoxin ejection (black and gray). *B*: each panel from top to bottom gives summary statistics for the number of spikes, the peak firing rate, and the latency to the 1st spike after the onset of recession, respectively (obtained from *A*). In each case, mean values over 10 trials are plotted as a function of the kinematical parameter  $l/v|$ . Black and gray bars correspond to trials before and after picrotoxin ejection, respectively. Error bars denote SD.

responses of the LGMD in all three cases, suggesting a preponderant role of feed-forward inhibition in shaping the neuron's responses under normal conditions. By using approaching and receding stimuli with different kinematic properties, we were able to shed light on the dynamic interaction between excitation and feed-forward inhibition within the LGMD's dendritic arborizations. Our results provide strong evidence for a precise timing and parallel time course of their relative activation. These results set new constraints on the biophysical factors shaping the receptive field properties of the LGMD to looming and receding stimuli.

#### Effects of picrotoxin on the membrane potential and firing rate of the LGMD

In control conditions, the membrane potential of the LGMD usually showed an abrupt repolarization after the cessation of object motion at the end of approach (Fig. 2*A*, shaded area). The temporal dynamics of repolarization was similar to that observed after activation of feed-forward inhibition by the fast flow stimulus during looming in the same neurons (Fig. 3*a* from Gabbiani et al. 2002). It is also consistent with the time course of IPSPs measured in the LGMD in response to the fast flow stimulus alone (Fig. 2*B*). These observations suggest that IPSPs contribute to the repolarization of the membrane poten-

tial at the end of stimulation. Similar observations have been made in previous intracellular recordings of the LGMD in response to looming (Figs. 1 and 3 in Rind 1996). Consistent with these observations, the repolarization of the LGMD membrane potential slowed down after ejection of picrotoxin into the lobula (Fig. 2*B*).

Local ejection of picrotoxin on the dorsal lobula, where the LGMD's inhibitory dendritic subfields are located, had significant effects both on the time course of the membrane potential and the instantaneous firing rate during looming. In contrast, picrotoxin application elicited only weak changes in the activity of units recorded in the medulla, the neuropil immediately presynaptic to the lobula (Fig. 2*C*). These results suggest that the effect of picrotoxin was sufficiently localized and that the changes observed with the LGMD were predominantly due to postsynaptic block of GABA<sub>A</sub> receptors. The excitatory dendritic subfield of the LGMD receives cholinergic inputs from retinotopic afferents and the presynaptic contacts thought to mediate lateral inhibition between such neighboring afferents in the lobula are also cholinergic (Rind and Simmons 1998). Therefore we conclude that picrotoxin specifically blocked inhibitory feed-forward inputs to the two inhibitory dendritic subfields of the LGMD.

The difference in membrane potential between picrotoxin and control conditions turned out to be a less-sensitive measure of the activation of feed-forward inhibition than the difference in instantaneous firing rate (Fig. 3). Our intracellular recordings were always performed in the dendritic tree of the LGMD at a significant electrotonic distance from the spike initiation zone as may be inferred from the reduced size of action potentials in Fig. 2*A* (compare, e.g., with Fig. 4*a* of Gabbiani et al. 2002). At these dendritic locations, the membrane potential is less tightly coupled to the instantaneous firing rate and may be significantly influenced by synaptic inputs. Thus during the early phases of looming, the membrane potential typically fluctuated rapidly between single spikes or spike bursts, both in control and picrotoxin conditions as is evident for instance in Fig. 2. The variability of these fluctuations across trials is therefore a likely cause for the decrease in sensitivity observed for membrane potential differences compared with instantaneous firing rate differences. Intracellular recordings close to the spike initiation zone may yield a sensitivity comparable to that observed at the level of firing rates. These recordings are technically more difficult because of the smaller size of the axon relative to that of the main dendritic compartments of the LGMD. Alternatively, voltage-clamp techniques similar to those developed by Borg-Graham et al. (1998) might prove useful to monitor directly changes in membrane conductance caused by feed-forward inhibition.

#### Activation of feed-forward inhibition during looming

A comparison of the instantaneous firing rate in control and picrotoxin conditions revealed that activation of feed-forward inhibition is delayed with respect to excitation, but otherwise follows a similar time course (Fig. 3). On average, a significant activation of feed-forward inhibition was detected early during the trials, when the objects approached  $\sim 23^\circ$  in size and well in advance of response termination (Figs. 2 and 3). This finding is consistent with observations by Rowell et al. (1977), showing that feed-forward inhibition can be activated by small field

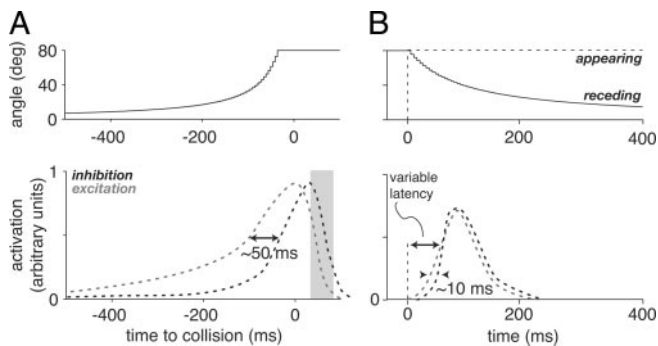


FIG. 8. Relative time course of activation of excitation and feed-forward inhibition for approaching, receding, and suddenly appearing objects as inferred from the experimental data. *A*: excitation and inhibition are activated in parallel during approach with excitation leading inhibition by  $\sim 50$  ms. In control conditions, inhibition becomes only apparent during response termination as excitation decays earlier and faster than inhibition (shaded area). The relative strength of inhibition relative to excitation is expected to increase faster with angular size at high  $l/|v|$  values, to account for faster response termination (Figs. 3 and 4). *B*: in response to receding stimuli, excitation is sharply activated, followed by delayed inhibition. This leads to a short summation time window ( $\sim 10$  ms) during which 1–2 spikes are reliably emitted. Thereafter inhibition is expected to hover roughly at the same level as excitation because additional spikes are sporadically emitted in response to the stimulus. A similar activation pattern is expected for suddenly appearing objects. However, excitation is likely to be activated less sharply, as the probability of spiking at the onset of the stimulus is decreased. The absolute activation level is expected to be smaller than for approaching objects.

stimuli. In contrast, a different presynaptic, lateral inhibitory process to the LGMD becomes ineffective beyond those angles (Gabbiani et al. 2002, their Fig. 3). Thus our experiments reveal that in control conditions excitation actually masks an increasingly large concurrent recruitment of feed-forward inhibitory inputs, as summarized in Fig. 8*A*. This finding resembles observations made in directionally selective V1 simple cells, where motion in the preferred direction is often reported to cause a large activation of both excitation and delayed inhibition when compared with the null direction (Monier et al. 2003; Priebe and Ferster 2005). Concurrent activation of excitation and inhibition has also been reported for preferred and null direction motion in fly lobula plate motion-sensitive tangential neurons (Single et al. 1997).

The experiments in which looming stimuli stopped at different final angles showed that the increase in excitation caused by larger final sizes was very effectively controlled by feed-forward inhibition. Indeed the number of spikes, peak firing rates, and peak firing times changed only slightly for angular sizes in excess of  $20^\circ$ , i.e., beyond the effective activation threshold for feed-forward inhibition (Fig. 4). Thus the concurrent increase in excitation and feed-forward inhibition is remarkably well balanced over the course of object approach. Further, these experiments show that the termination of the response is affected by the kinematic parameter of the stimuli. For high values of  $l/|v|$ , the angular size of the approaching object increases more slowly, presumably causing a slower and weaker activation of excitation that is overcome earlier by inhibition as final angular size increases from  $20$  to  $80^\circ$ . This hypothesis was confirmed by subsequent picrotoxin ejection experiments because after block of feed-forward inhibition, the  $l/|v|$  dependence of response termination on final angle was abolished (Fig. 5).

### Preferential tuning of excitation and feed-forward inhibition for approaching objects

The responses of the LGMD/DCMD to a square suddenly appearing on the screen were typically weak, except at the smallest object size ( $20^\circ$ ) which, according to our previous experiments, was below the threshold for significant activation of feed-forward inhibition. Interestingly, the latency of the response decreased with object size in exactly the same way both before and after picrotoxin application. This demonstrates directly the tight relation between the activation of excitation and feed-forward inhibition with varying object size under these experimental conditions. Similar observations were made for the response onset to object recession (Fig. 6*B*).

In control conditions, the responses to object recession had similar characteristics to those reported by Rind (1996). The precise timing of spikes observed at the onset of recession was presumably due to the short delay between the activation of excitation and feed-forward inhibition similar to that observed in Fig. 2*B* for the fast flow stimulus (see also Fig. 8*B*). Thus feed-forward inhibition decreases the temporal summation window for excitatory inputs (Mittmann et al. 2005; Perez-Orive et al. 2002; Pouille and Scanziani 2001). After picrotoxin ejection, both peak firing rates and mean spike counts increased, confirming the role of feed-forward inhibition in terminating the responses to receding stimuli (Rind 1996). Thus feed-forward inhibition plays a role in shaping the preferential tuning of the LGMD to approaching versus receding stimuli. However, even after picrotoxin ejection, peak firing rates and mean spike counts were well below those obtained for inverted sequences of approaching stimuli with the same  $l/|v|$  value. Further, no obvious changes in the dynamical interplay of excitation and inhibition were revealed by varying  $l/|v|$  (Fig. 7) in contrast to approaching sequences. These results suggest that both excitation and feed-forward inhibition are weaker for receding than approaching stimuli and that they show little dependence on the kinematics of recession. The weaker activation of excitation for receding stimuli might be due to lateral inhibition between adjacent excitatory afferents mediated by muscarinic acetylcholine receptors (Rind and Bramwell 1996). The mechanism responsible for weaker activation of feed-forward inhibition is presently unknown.

### Implications for biophysical modeling of LGMD responses to looming stimuli

These results have implications for modeling the responses of the LGMD to looming and receding stimuli. In an earlier biophysical model of the LGMD, for example, Rind and Bramwell (1996) assumed that activation of feed-forward inhibition occurs only at the last stages of object approach (e.g., their Fig. 4). Their model assumed instead a significant effect of lateral inhibition during most of the approach sequence. On the contrary, as described in Gabbiani et al. (2002), activation of lateral inhibition is ineffective at controlling excitation beyond  $\sim 23^\circ$ , and, according to the present results, feed-forward inhibition is significantly activated for angular sizes in excess of  $23^\circ$ , that is, over a large fraction of a looming trial. The response properties of the LGMD over a wide range of  $l/|v|$  values and final angles, as gathered here, should provide an effective way to constrain the relative activation of excitation

and feed-forward inhibition onto the LGMD in a biophysical model. Thus future biophysical models of the LGMD will need to take into account current constraints on the dynamics of excitation and feed-forward inhibition as well as recently derived constraints on the spatial receptive field properties of the LGMD (Krapp and Gabbiani 2005). These models are in turn likely to provide important constraints on the biophysical mechanisms underlying the sensitivity of the LGMD to looming stimuli and the multiplicative interaction between excitation and feed-forward inhibition characterized in earlier experiments (Gabbiani et al. 2002, 2004).

## ACKNOWLEDGMENTS

Use of the QNX 6 operating system was made possible through the Educational Program of QNX Software Systems. Thanks to Dr. H.G. Krapp for comments on the manuscript.

## GRANTS

This work was supported by the National Institutes of Health and an Alfred P. Sloan Fellowship to F. Gabbiani. Multichannel silicon probes were provided by the University of Michigan Center for Neural Communication Technology sponsored by Division of Research Resources Grant P41-RR-09754.

## REFERENCES

- Anderson JS, Carandini M, and Ferster D. Orientation tuning of input conductance, excitation, and inhibition in cat primary visual cortex. *J Neurophysiol* 84: 909–926, 2000.
- Borg-Graham LJ, Monier C, and Frégnac Y. Visual input evokes transient and strong shunting inhibition in visual cortical neurons. *Nature* 393: 369–73, 1998.
- Chance FS, Abbott LF, and Reyes AD. Gain modulation from background synaptic input. *Neuron* 35: 773–782, 2002.
- Cohen I and Gabbiani F. Multi-electrode extracellular recordings from the locust optic lobe. *Soc Neurosci Abstr* 491.4, 2003.
- Cohen I and Miles R. Contributions of intrinsic and synaptic activities to the generation of neuronal discharges in in vitro hippocampus. *J Physiol* 524: 485–502, 2000.
- Cooke DF and Graziano MS. Super-flinchers and nerves of steel: defensive movements altered by chemical manipulation of a cortical area. *Neuron* 43: 585–593, 2004.
- Elphick M, Williams L, and O'Shea M. New features of the locust optic lobe: evidence of a role for nitric oxide in insect vision. *J Exp Biol* 199: 4139–4143, 1996.
- Fogassi L, Gallese V, Fadiga L, Luppino G, Matelli M, and Rizzolatti G. Coding of peripersonal space in inferior premotor cortex (area F4). *J Neurophysiol* 76: 141–157, 1996.
- Gabbiani F, Krapp HG, Hatsopoulos N, Mo CH, Koch C, and Laurent G. Multiplication and stimulus invariance in a looming-sensitive neuron. *J Physiol Paris* 98: 19–34, 2004.
- Gabbiani F, Krapp HG, Koch C, and Laurent G. Multiplicative computation in a visual neuron sensitive to looming. *Nature* 420: 320–324, 2002.
- Gabbiani F, Krapp HG, and Laurent G. Computation of object approach by a wide-field, motion-sensitive neuron. *J Neurosci* 19: 1122–1141, 1999.
- Gabbiani F, Mo C, and Laurent G. Invariance of angular threshold computation in a wide-field looming sensitive neuron. *J Neurosci* 21: 314–329, 2001.
- Hatsopoulos N, Gabbiani F, and Laurent G. Elementary computation of object approach by a wide-field visual neuron. *Science* 270: 1000–1003, 1995.
- Hirsch JA, Alonso JM, Reid RC, and Martinez LM. Synaptic integration in striate cortical simple cells. *J Neurosci* 18: 9517–9528, 1998.
- Holt GR and Koch C. Shunting inhibition does not have a divisive effect on firing rates. *Neural Comput* 9: 1001–1013, 1997.
- Kuhn A, Aertsen A, and Rotter S. Neuronal integration of synaptic input in the fluctuation-driven regime. *J Neurosci* 24: 2345–2356, 2004.
- Krapp HG and Gabbiani F. Spatial distribution of inputs and local receptive field properties of a wide-field looming-sensitive neuron. *J Neurophysiol* 93: 2240–2253, 2005.
- Lehmann EL. *Nonparametric Statistical Methods Based on Ranks*. Upper Saddle River, NJ: Prentice Hall, 1998.
- Matheson T, Krapp HG, and Rogers SM. Plasticity in the visual system is correlated with a change in lifestyle of solitary and gregarious locusts. *J Neurophysiol* 91: 1–12, 2004.
- Mickey RM, Dunn OJ and Clark V. *Applied Statistics: Analysis of Variance and Regression*. San Diego, CA: Wiley, 2004.
- Milton JS and Arnold JC. *Introduction to Probability and Statistics* (3rd ed.). New York: McGraw-Hill, 1995.
- Mittmann W, Koch U, and Hausser M. Feed-forward inhibition shapes the spike output of cerebellar Purkinje cells. *J Physiol* 563: 369–378, 2005.
- Monier C, Chavane F, Baudot P, Graham LJ, and Frégnac Y. Orientation and direction selectivity of synaptic inputs in visual cortical neurons: a diversity of combinations produces spike tuning. *Neuron* 37: 663–680, 2003.
- O'Shea M and Rowell CH. Protection from habituation by lateral inhibition. *Nature* 254: 53–55, 1975.
- O'Shea M and Williams JLD. The anatomy and output connection of a locust visual interneuron: the Lobular Giant Movement Detector (LGMD) neuron. *J Comp Physiol [A]* 91: 257–266, 1974.
- Perez-Orive J, Mazor O, Turner GC, Cassenaer S, Wilson RL, and Laurent G. Oscillations and sparsening of odor representation in the mushroom body. *Science* 297: 359–365, 2002.
- Pouille F and Scanziani M. Enforcement of temporal fidelity in pyramidal cells by somatic feed-forward inhibition. *Science* 293: 1159–1163, 2001.
- Pouzat C, Mazor O, and Laurent G. Using noise signature to optimize spike-sorting and to assess neuronal classification quality. *J Neurosci Methods* 122: 43–57, 2002.
- Priebe NJ and Ferster D. Direction selectivity of excitation and inhibition in simple cells of the cat primary visual cortex. *Neuron* 45: 133–145, 2005.
- Rauh JJ, Lummis SC, and Sattelle DB. Pharmacological and biochemical properties of insect GABA receptors. *Trends Pharmacol Sci* 11: 325–329, 1990.
- Rind FC. Intracellular characterization of neurons in the locust brain signaling impending collision. *J Neurophysiol* 75: 986–995, 1996.
- Rind FC and Bramwell DI. Neural network based on the input organization of an identified neuron signalling impending collision. *J Neurophysiol* 75: 967–985, 1996.
- Rind FC and Simmons PJ. Orthopteran DCMD neuron: a reevaluation of responses to moving objects. I. Selective responses to approaching objects. *J Neurophysiol* 68: 1654–1666, 1992.
- Rind FC and Simmons PJ. Local circuit for the computation of object approach by an identified visual neuron in the locust. *J Comp Neurol* 395: 405–415, 1998.
- Rowell CHF. The orthopteran descending movement detector (DMD) neurons: a characterization and review. *Z Vergl Physiol* 73: 167–194, 1971.
- Rowell CHF. Boredom and attention in a cell in the locust visual system. In: *Experimental Analysis of Insect Behavior*, edited by Browne LB. New York: Springer Verlag, 1974, p. 87–99.
- Rowell CH and O'Shea M. The neuronal basis of a sensory analyzer, the acridid movement detector system. III. Control of response amplitude by tonic lateral inhibition. *J Exp Biol* 65: 617–625, 1976.
- Rowell CH, O'Shea M, and Williams JLD. The neuronal basis of a sensory analyzer, the acridid movement detector system. IV. The preference for small field stimuli. *J Exp Biol* 68: 157–185, 1977.
- Schlotterer GR. Response of the locust descending movement detector neuron to rapidly approaching and withdrawing visual stimuli. *Can J Zool* 55: 1372–1376, 1977.
- Shepherd G. *The Synaptic Organization of the Brain* (5th ed.). Oxford, UK: Oxford Univ. Press, 2003.
- Single S, Haag J, and Borst A. Dendritic computation of direction selectivity and gain control in visual interneurons. *J Neurosci* 17: 6023–6030, 1997.
- Strausfeld NJ and Naessel DR. Neuroarchitectures serving compound eyes of crustacea and insects. In: *Handbook of Sensory Physiology*, vol. VII/7B, edited by Autrum H. Berlin: Springer, 1981, p. 1–132.
- Sun H and Frost BJ. Computation of different optical variables of looming objects in pigeon nucleus rotundus neurons. *Nat Neurosci* 1: 296–303, 1998.
- Warzecha AK, Egelhaaf M, and Borst A. Neural circuit tuning fly visual interneurons to motion of small objects. I. Dissection of the circuit by pharmacological and photoinactivation methods. *J Neurophysiol* 69: 329–339, 1993.
- Wicklein M and Strausfeld NJ. Organization and significance of neurons that detect change of visual depth in the hawk moth *Manduca sexta*. *J Comp Neurol* 424: 356–376, 2000.
- Wilson M. Angular sensitivity of light and dark adapted locust retinula cells. *J Comp Physiol* 97: 323–328, 1975.